

Engineering of NADPH Supply Boosts Photosynthesis-Driven Biotransformations

Leen Assil-Companiononi,[#] Hanna C. Büchenschütz,[#] Dániel Solymosi, Nina G. Dyczmons-Nowaczyk, Kristin K. F. Bauer, Silvia Wallner, Peter Macheroux, Yagut Allahverdiyeva, Marc M. Nowaczyk,^{*} and Robert Kourist^{*}



Cite This: *ACS Catal.* 2020, 10, 11864–11877



Read Online

ACCESS |



Metrics & More



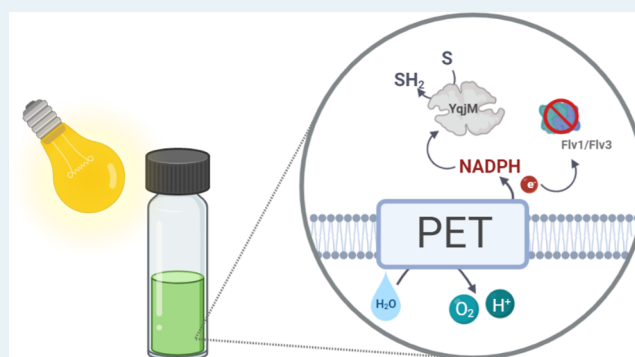
Article Recommendations



Supporting Information

ABSTRACT: Light-driven biocatalysis in recombinant cyanobacteria provides highly atom-efficient cofactor regeneration *via* photosynthesis, thereby remediating constraints associated with sacrificial cosubstrates. However, despite the remarkable specific activities of photobiocatalysts, self-shading at moderate-high cell densities limits efficient space-time-yields of heterologous enzymatic reactions. Moreover, efficient integration of an artificial electron sink into the tightly regulated network of cyanobacterial electron pathways can be highly challenging. Here, we used C=C bond reduction of 2-methylmaleimide by the NADPH-dependent ene-reductase YqjM as a model reaction for light-dependent biotransformations. Time-resolved NADPH fluorescence spectroscopy allowed direct monitoring of in-cell YqjM activity and revealed differences in NADPH steady-state levels and oxidation kinetics between different genetic constructs. This effect correlates with specific activities of whole-cells, which demonstrated conversions of >99%. Further channelling of electrons toward heterologous YqjM by inactivation of the flavodiiron proteins (Flv1/Flv3) led to a 2-fold improvement in specific activity at moderate cell densities, thereby elucidating the possibility of accelerating light-driven biotransformations by the removal of natural competing electron sinks. In the best case, an initial product formation rate of 18.3 mmol h⁻¹ L⁻¹ was reached, allowing the complete conversion of a 60 mM substrate solution within 4 h.

KEYWORDS: light-driven biotransformations, electron channeling, NADPH fluorescence, photocatalysis, photosynthesis, flavodiiron proteins, cyanobacteria, *Synechocystis*



Genetically engineered photoautotrophic organisms have emerged as possible hosts for the future production of biobased chemicals devoid of land-use conflicts for agricultural purposes.^{1,2} Algae and cyanobacteria have been applied for the production of food additives^{3,4} and feed,⁵ with metabolic engineering further expanding their potential for the production of various chemicals such as terpenoids,⁶ alcohols,^{7,8} and sugars.^{9,10}

The utilization of photoautotrophs for biotechnology provides several advantages such as the capacity to fix carbon dioxide and utilize photosynthetically derived redox power. Furthermore, photosynthetic cells offer specific benefits including an NADPH-based metabolism¹¹ and *in situ* oxygen production.^{12,13} However, despite these benefits, inadequate light availability limits the growth of suspension cultures to a few grams per liter.¹⁴ This occurs due to *self-shading*—a phenomenon where growing cells conceal each other, thereby leading to uneven and inadequate light distribution.¹⁵ Consequently, a considerable increase of photoautotrophic

production rates is crucial to compete with highly optimized heterotrophic production systems.

Using the photosynthetic pool of reducing equivalents, in the form of reduced ferredoxin (Fd) or NADPH for reductive biotransformations (Figure 1), allows one to overcome the poor atom economy (i.e., conversion efficiency of a chemical process accounting for all atoms involved) associated with the use of sacrificial organic cosubstrates, such as hydrogen,¹⁶ which is a limitation commonly associated with biocatalytic redox reactions. The work by Kuk et al. serves as an example where water was used as an electron donor to produce NADH for the reduction of CO₂ to methanol.¹⁷ Furthermore, the

Received: June 13, 2020

Revised: September 4, 2020

Published: September 4, 2020



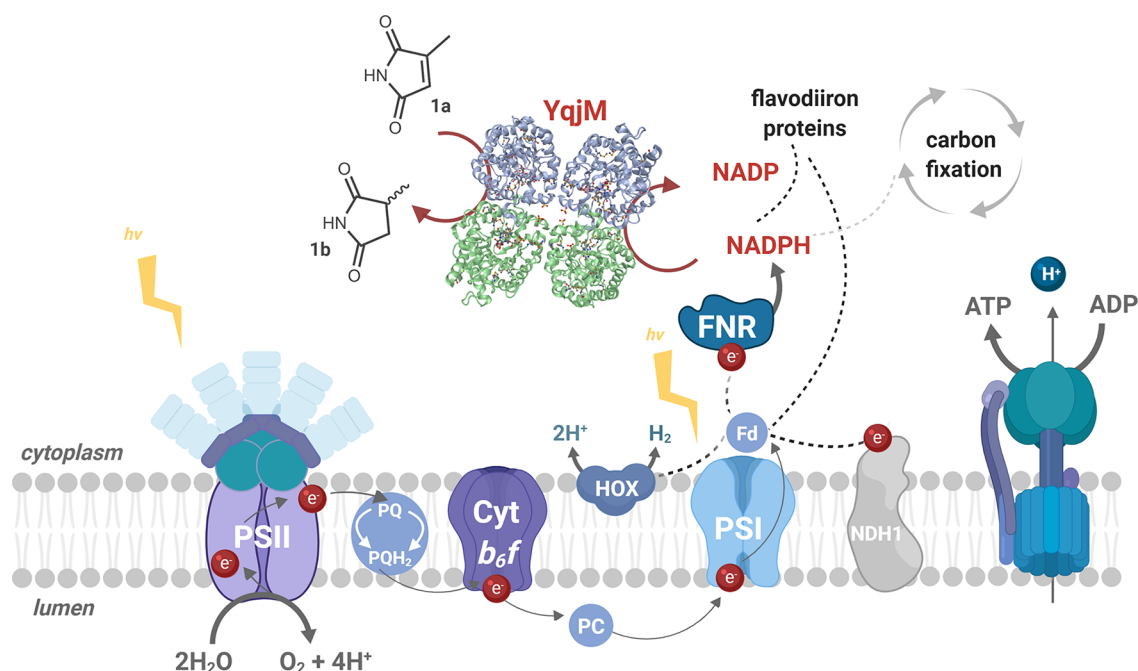


Figure 1. Simplified representation of the photosynthetic electron transport (PET) chain in *Synechocystis* depicting the introduction of the heterologous ene-reductase, YqjM (PDB ID: 1Z41).²² NADPH, a primary photosynthetic reductant, mainly produced via linear PET, involves three major photosynthetic complexes, PSII, Cytochrome (Cyt) b₆f, and PSI. PSII drives water oxidation on the luminal side of the thylakoid membrane using light energy. The electrons extracted from water travel via several redox cofactors to plastoquinone (PQ) pool, Cytb₆f, plastocyanin/Cytc6, PSI and end up reducing Fd. Fd is eventually oxidized by Fd-NADP⁺ reductase (FNR) to generate NADPH. Depicted above are examples of naturally occurring electron sinks such as the bidirectional hydrogenase (HOX), type I NADH dehydrogenase (NDH1), and flavodiiron proteins. YqjM constitutes a strong, yet tunable electron sink which can be suddenly activated through the introduction of a substrate, 2-methylmaleimide (1a) that is converted to 2-methylsuccinimide (1b). **Other abbreviations** PQH₂: plastoquinol, PC: plastocyanin. Image created using BioRender.

work of Nakamura et al. and Hölsch et al. helped establish the concept of using a photosynthetically derived pool of reductants with the use of wildtype cyanobacteria for the reduction of aryl ketones.^{18–20}

We have previously expanded this approach with a proof-of-concept study in *Synechocystis* sp. PCC 6803 (hereafter *Synechocystis* or Syn) by introducing the NAD(P)H dependent ene-reductase YqjM^{21,22} from *Bacillus subtilis*. With this system, we achieved product formation rates of 10 mM h⁻¹ for the conversion of 2-methylmaleimide (1a) to 2-methylsuccinimide (1b).¹¹ Light-driven whole-cell biotransformations with other oxidoreductases, such as monooxygenases, alcohol dehydrogenases, and imine reductases, have also been reported by us and others.^{13,23–25} Thus far, the highest specific activities reported in *Synechocystis* are those of the ene-reductase YqjM, indicating that it behaves as a strong electron sink drawing photosynthetically derived electrons.

In *Synechocystis*, the photosynthetic reducing power is required for a wide range of metabolic processes such as carbon fixation and the assimilation of nitrate and sulfur.^{26,27} However, if the supply of energy-rich electrons exceeds demand, the photosynthetic apparatus is protected by alternative electron sinks like flavodiiron proteins (FDPs). These proteins transfer excess electrons from NAD(P)H^{28,29} or reduced Fd^{30–32} to oxygen, thus generating a water–water cycle.³³ The Flv1/Flv3 hetero-oligomer is, therefore, indispensable for the survival of cyanobacteria and green algae under fluctuating light intensities.^{34,35} Under specific conditions, these proteins act as a very strong electron sink, redirecting up to 40–60% of electrons originating from

photosystem (PS) II water-splitting to oxygen.^{36,37} Under controlled laboratory conditions, these photoprotective processes may no longer be needed, potentially opening the possibility of redirecting electrons toward a desired process and thus alleviating the effects of self-shading.

Previously, enhanced activity of a heterologous cytochrome P450 monooxygenase was demonstrated through the disruption of a competing pathway by deleting a type I NADH dehydrogenase complex (NDH-1) subunit in *Synechococcus* sp. PCC 7002.³⁸ Similar methods have also been reported for other purposes including the production of sucrose and photohydrogen.^{39,40}

Herein, we investigate the effect of the NADPH-pool as a possible bottleneck for light-driven biotransformations using the stereoselective reduction of 1a catalyzed by the ene-reductase YqjM as a model. The extent to which productivity and space-time-yields can be accelerated under self-shading conditions, where NADPH production may be compromised, is also studied by the deletion of the Flv1/Flv3 oligomer.

RESULTS

Promoter Engineering Is Effective for Productivity Enhancement. In previous work,²³ the effect of the promoter used for the expression of a heterologous gene of an imine reductase proved to be crucial for an activity increase of the whole-cell cyanobacterial biocatalyst. We, therefore, investigated the effects of three different promoters in order to elucidate their effects on the expression of YqjM and its activity. The inducible, Zn²⁺-dependent promoter P_{zia}^{41,42} was expected to produce lower amounts of protein in comparison

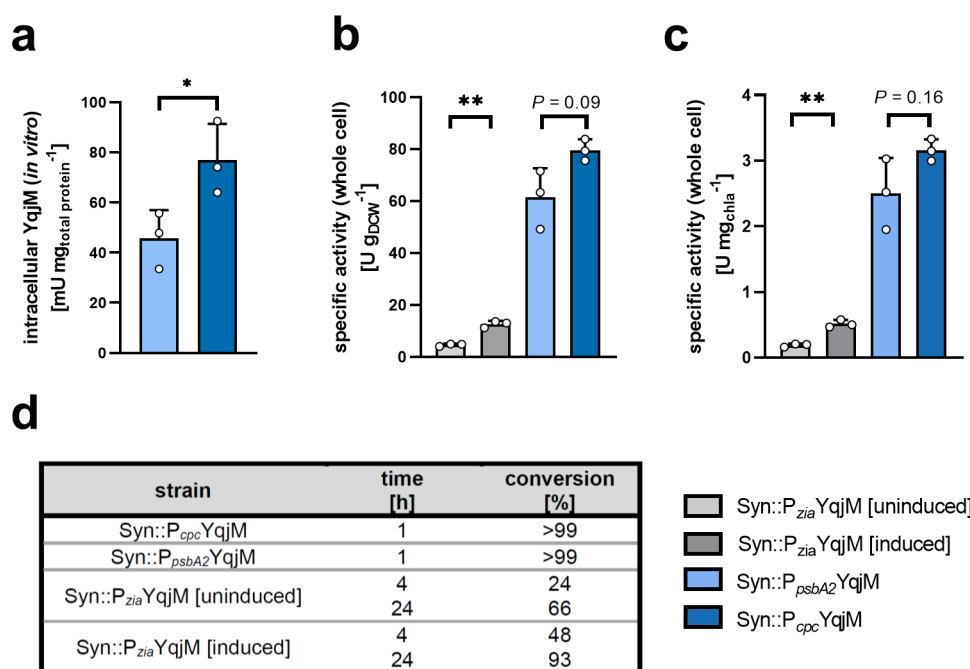


Figure 2. YqjM-mediated biotransformations of the substrate **1a** (10 mM) using whole *Synechocystis* cells under the control of different promoters after cultivation under standard conditions. (for more details please refer to the **Materials and Methods** section). [a] shows *in vitro* quantified active YqjM activity, relative to total protein, in strains carrying P_{cpc}::YqjM and P_{psbA2}::YqjM cassettes (this activity could not be determined in strains with the P_{zia}::YqjM cassette). [b] and [c] show specific whole cell activities relative to cell density and chlorophyll *a* (*chl_a*) content, respectively. [d] shows conversion levels of **1a** to the product **1b**. Reactions were performed at a light intensity of 150 μE m⁻² s⁻¹. Data includes values from biological replicates (*N* = 3) ± SD. *P* values were calculated using Welch's *t* test (**P* < 0.05, ***P* < 0.001) and their exact values, where asterisks are placed, can be found in the raw data files.

to the light-induced promoter P_{psbA2} and the partially light-regulated promoter P_{cpc}. Wildtype *Synechocystis* and transgenic strains constructed in this work and previous work¹¹ were used (SI, Table S1). We were able to detect intracellular *in vitro* YqjM activities in Syn::P_{psbA2}:YqjM and Syn::P_{cpc}:YqjM; however, no such activity was detected in Syn::P_{zia}:YqjM (Figure 2a). This observation was further sustained by SDS-PAGE analysis which yielded discernible YqjM bands under the control of P_{psbA2} and P_{cpc} but not P_{zia} (SI, Figure S1). Next, we investigated the YqjM-mediated biotransformation of **1a** in the engineered whole cells with these different promoters to assess specific initial activities.

Using cells grown under standard conditions (described in the **Materials and Methods** section), Syn::P_{cpc}:YqjM and Syn::P_{psbA2}:YqjM both catalyzed the conversion of 10 mM **1a** to completion within 1 h. In these whole-cell biotransformations, Syn::P_{cpc}:YqjM exhibited a 1.3-times (±0.16) faster initial activity compared with Syn::P_{psbA2}:YqjM based on dry cell weight (DCW) and chlorophyll *a* (*chl_a*) content (Figure 2b,c). This difference, however, did not correspond with the 1.7-times (±0.45) higher amount of active enzyme in the crude cell extract determined in an *in vitro* activity assay (Figure 2a). Although this difference is not statistically significant, we nonetheless believe that this suggests that whole-cell biotransformations are limited by factors other than the intracellular concentration of the oxidoreductase. As the availability of the redox factor is an obvious limiting factor, we set out to measure the kinetic parameters of the enzyme toward both the substrate and NADPH and determine a possible reducing effect of the biotransformation on intracellular NADPH.

NADPH Is a Limiting Factor for the YqjM Reaction.

In order to investigate the possible limiting role of the redox cofactor on the enzymatic reaction, we sought to determine the kinetic parameters of the reductive and oxidative half reactions in presteady state measurements of purified YqjM in stop-flow experiments. First, the reduction of the flavin cofactor was determined as a function of the concentration of either NADPH or NADH. In both cases, we observed saturation behavior with a maximal velocity of k_{red} of $12.58 \pm 1.06 \text{ s}^{-1}$ and $0.97 \pm 0.03 \text{ s}^{-1}$ for NADPH and NADH, respectively (Figure 3a,b). From these data, we deduced K_D -values of 39.8 ± 7.1 and $140.4 \pm 24.5 \text{ μM}$ for NADPH and NADH, respectively—these values clearly show that NADPH is the preferred substrate. Second, the oxidative rate of YqjM was determined using **1a** as an electron-accepting substrate (Figure 3c). In contrast to the reductive half reaction, the observed rate of oxidation increased linearly with higher substrate concentrations reaching a k_{obs} of 500 s⁻¹ at 250 μM **1a**. Higher concentrations of this substrate could not be analyzed because faster rates could not be reliably measured in our experimental setup.

The kinetics revealed that **1a** is an extremely efficient substrate for YqjM, where at concentrations of 250 μM, the observed k_{obs} of 500 s⁻¹ shows that the oxidative half-reaction is at least 50-fold faster than the reductive half-reaction (Figure 3c). Our measurements also reveal that for concentrations ≥ 500 μM NADPH, cofactor reduction occurs at maximal velocity (Figure 3a). Thus, an intracellular NADPH concentration higher than 500 μM, would not lead to an increase in cellular turnover. However, if NADPH is depleted and drops significantly below 200 μM, a strong effect on k_{obs} can be observed (Figure 3a).

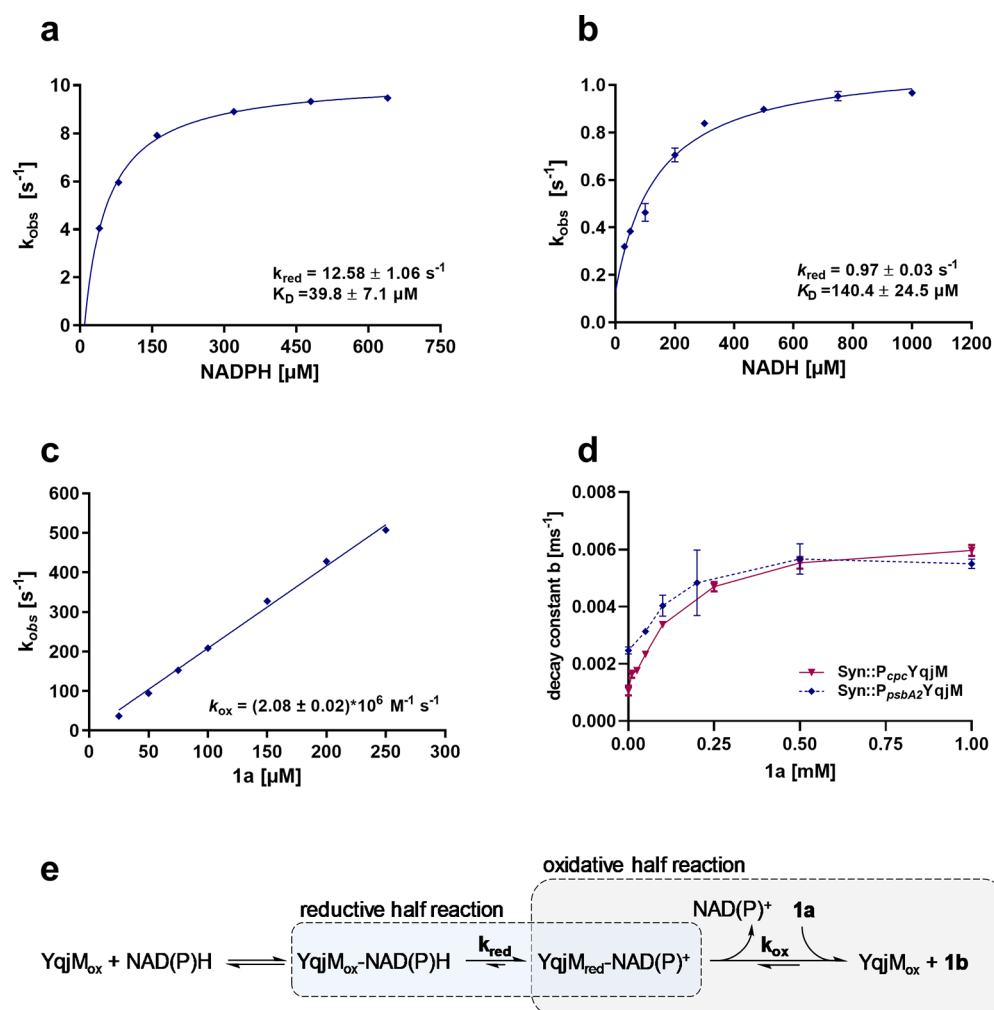


Figure 3. Determination of the reductive rate of purified YqjM with [a] NADPH and [b] NADH as reducing agents. [c] Determination of the oxidative rate of YqjM with 1a as substrate and 1b as reduced product. [a], [b], and [c] were determined using purified enzyme, and their corresponding equations are shown. Panel [d] depicts the decay constant b of $\text{Syn}::P_{\text{cpc}}\text{YqjM}$ and $\text{Syn}::P_{\text{psbA2}}\text{YqjM}$ with different 1a concentrations up to 1 mM; these values were determined in whole-cells using fluorescence spectroscopy. Data plotted is derived from biological replicates ($N = 3$) \pm SD. Panel [e] shows the reductive and oxidative half reactions of YqjM.

The data presented clearly indicate that the reductive half reaction is the rate limiting step for enzymatic activity, which strengthens the assumption that the supply of reduced nicotinamide cofactors might be a limiting factor for light-driven ene-reduction. In order to exclude substrate limitation, we also conducted whole cell NADPH decay measurements (described in the following section) using different substrate concentrations and found saturation above 0.5 mM (Figure 3d), which ruled out a limiting role of substrate transport and supported our conclusions from the enzyme kinetics. Therefore, the supply of NADPH appeared to be a limiting factor for the ene-reduction.

Heterologous Ene-Reductions Decrease Intracellular NADPH Levels. To the best of our knowledge, NAD(P)H-availability in light-driven biotransformations has never been investigated before. The fast C=C double-bond reduction by YqjM in recombinant *Synechocystis* is a suitable model for investigations.

Fast changes (\sim s) in the redox state of the intracellular NADP pool can be monitored by pulse amplitude modulated (PAM) fluorescence spectroscopy. We applied this spectroscopic tool to compare the NADPH steady-state levels and

oxidation kinetics after light-to-dark transition between the WT and the three engineered strains ($\text{Syn}::P_{\text{zia}}\text{YqjM}$, $\text{Syn}::P_{\text{psbA2}}\text{YqjM}$ and $\text{Syn}::P_{\text{cpc}}\text{YqjM}$) in the presence and absence of 1a (Figure 4a). WT cells showed a steady-state fluorescence level during illumination with actinic light for 20 s that corresponds to constant NADP^+ reduction by the PET and concomitant NADPH reoxidation by downstream processes such as CO_2 fixation as well as nitrate and sulfur assimilation. The relatively small NADP^+ pool ($\sim 8 \text{ NADP}^+$ per PSI according to Kauny and Sétif⁴³) is highly reduced under these conditions because of efficient PET. After switching off actinic light, the NADPH fluorescence signal rapidly decays ($\sim 3 \text{ s}$) to a temporary minimum that reflects a more oxidized NADP^+ pool. The addition of 1a to WT cells changes the steady-levels or decay kinetics only slightly (Figure 4b,c), which indicates minimal background reactions and excludes interference of the fluorescence assay with the model substrate, 1a, for YqjM-dependent reactions.

Heterologous expression of YqjM under the control of the inducible P_{zia} promoter revealed no statistically significant difference in the NADPH steady-levels or decay kinetics with or without the addition of 1a, which is consistent with the low

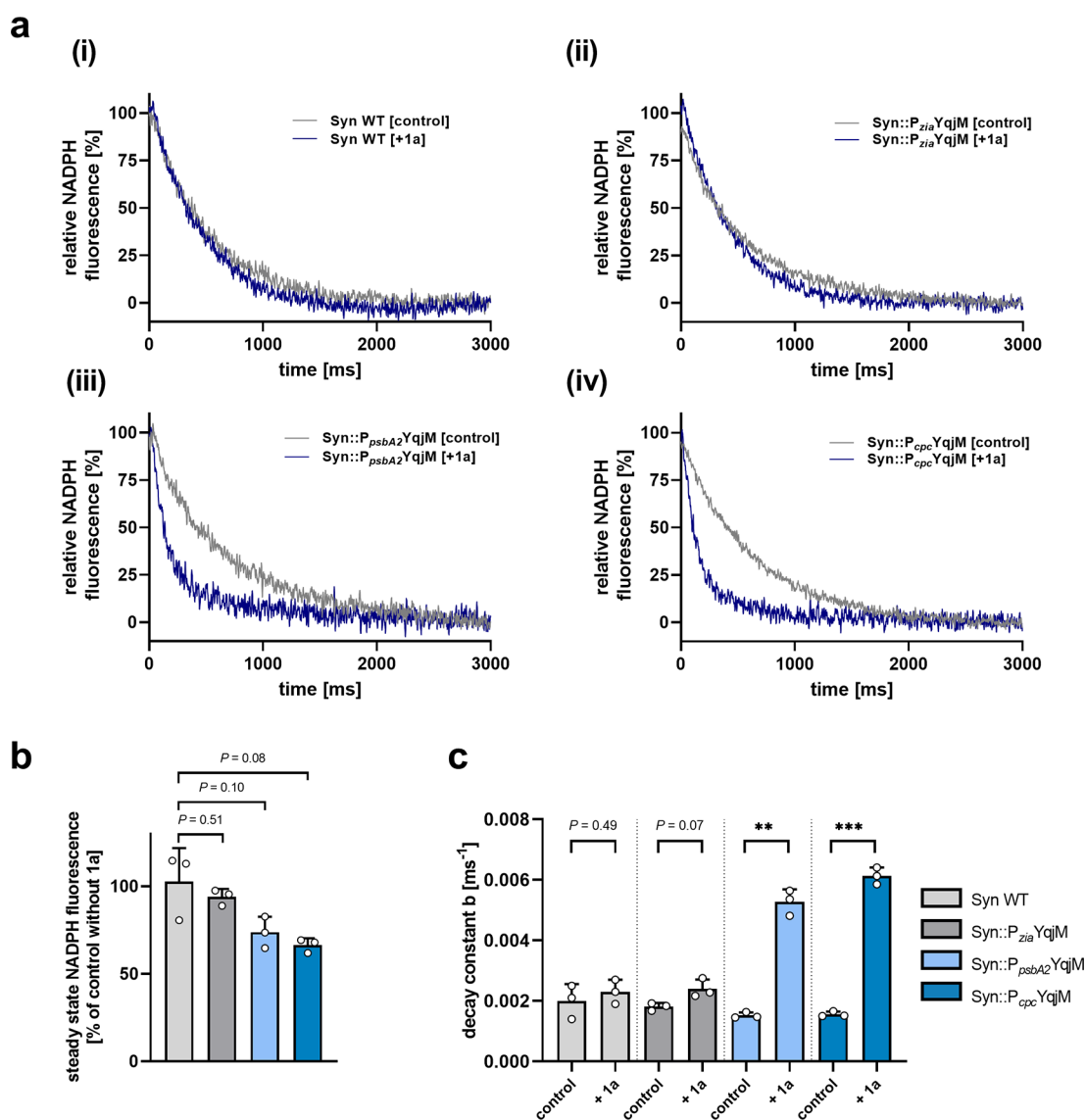


Figure 4. NADPH-fluorescence measurements after cultivation at a light intensity of $50 \mu\text{E m}^{-2} \text{s}^{-1}$ showing [a] the experimental NADPH decay in (i) Syn WT, (ii) Syn::P_{zia}YqjM, (iii) Syn::P_{psbA2}YqjM and (iv) Syn::P_{cpc}YqjM cells ($\text{OD}_{750} = 1$). The gray lines [control] indicate decays in the absence of substrate, the blue [2MM] lines show decays in the presence of the substrate **1a**. The time 0 ms indicates the point at which the lights are switched off. Curves were normalized to zero at 3 s. [b] depicts the steady-state values during illumination of the strains. [c] shows the decay constants of the respective strains with and without the addition of **1a** (1 mM). Bars include data from three measurements \pm SD with individual values depicted. *P* values were calculated using Welch's *t* test (***P* < 0.01, ****P* < 0.001). Exact *P* values where asterisks are placed can be found in the raw data files.

intracellular enzyme concentration and slow whole-cell activity of the corresponding cells (Figure 2). Conversely, the strength of the P_{psbA2} and P_{cpc} promoters, which led to high intracellular levels of YqjM and fast conversion activity of the corresponding cells (Figure 2), is also reflected by the NADPH fluorescence measurements (Figure 4). The addition of **1a** (1 mM) lowered the steady-state NADPH fluorescence level in the light by $\sim 30\%$ in both mutant lines due to increased NADPH consumption by YqjM. The effect might be more complex, as the dark state, which we used for normalization of the data in all graphs, might not reflect a fully oxidized NADP⁺ pool and may also change because of **1a** related NADPH consumption in the dark. However, the prompt and fast fluorescence decay upon light-to-dark transition indicates that NADPH is mainly responsible for the signal. This fluorescence decay is ~ 3 times faster in the

Syn::P_{psbA2}YqjM and Syn::P_{cpc}YqjM cells after the addition of **1a**, which also indicates an efficient flux of NADPH to YqjM.

2-Methylmaleimide Toxicity Is Mitigated by YqjM Expression. Maleimides are known to form stable thioether bonds with free sulfhydryl groups of cysteine amino acid residues. As several vital photosynthetic proteins contain cysteine,⁴⁴ thioesterisation potentially compromises their function. Therefore, we investigated the effects of **1a** on the photosynthetic machinery of Syn WT, Syn::P_{cpc}YqjM, ΔFlv1 , and $\Delta\text{Flv1}::\text{P}_{\text{cpc}}\text{YqjM}$. The effective yields of PSI and PSII (Y(I) and Y(II), respectively) were assessed by probing whole cell chlorophyll fluorescence indicative for PSII and determining absorbance of the PSI reaction center P700 (Figure 5, Figure S4). Syn WT and the mutant strains Syn::P_{cpc}YqjM, ΔFlv1 , and $\Delta\text{Flv1}::\text{P}_{\text{cpc}}\text{YqjM}$ demonstrated comparable Y(I) (Figure 5a, without **1a**) and Y(II) (Figure 5b, without **1a**)

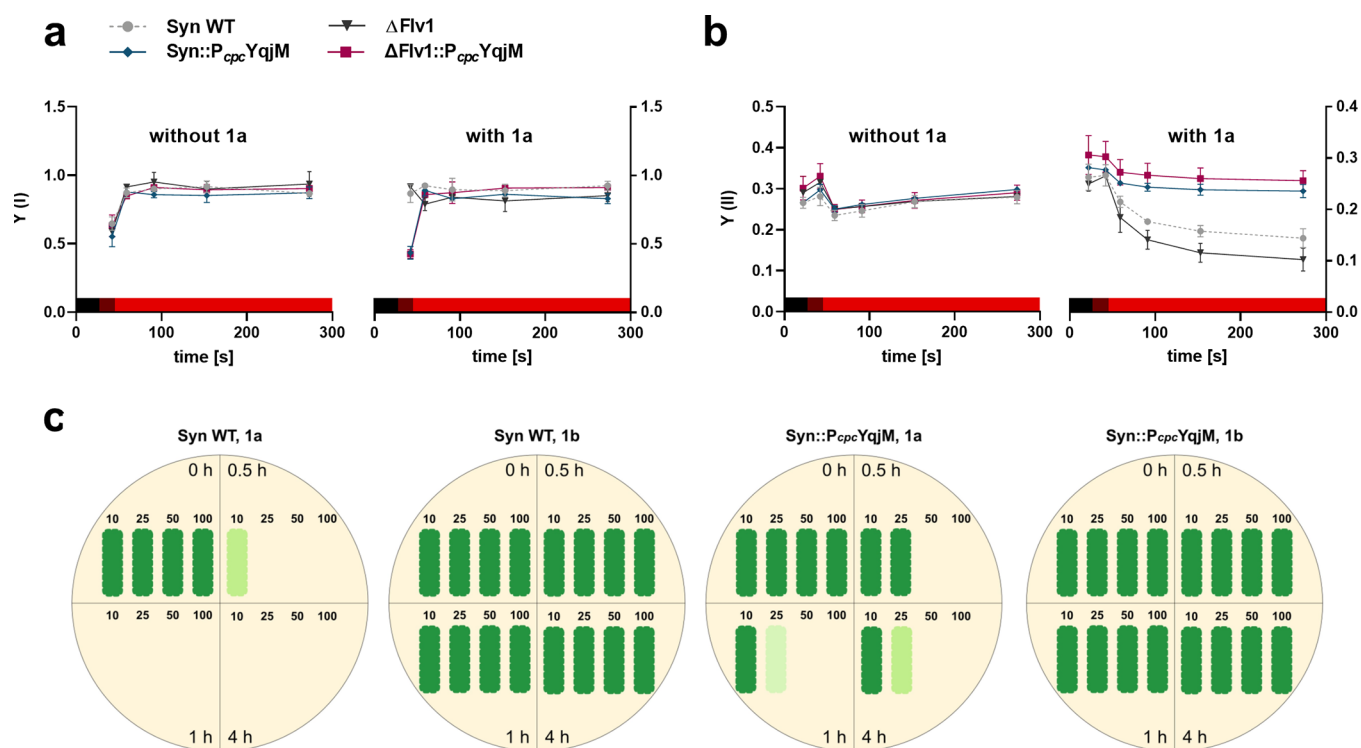


Figure 5. Yield of [a] PSI and [b] PSII without and with **1a** (10 mM). Colored bar represents light conditions during the respective times (black: dark, dark red: far red light, red: red light). Values plotted represent averages derived from biological replicates ($N = 2$) \pm SD. [c] Shows a schematic representation of the viability tests performed on Syn WT and Syn::P_{cpc}YqjM with the original images presented in Figure S5 of the SI. For the tests, either the substrate or product were added at final concentrations of 10, 25, 50, and 100 mM. Cells used for the viability test were cultured under standard cultivation conditions ($60 \mu\text{E m}^{-2} \text{s}^{-1}$, $30 \text{ }^\circ\text{C}$) with the reactions themselves carried out with a light intensity of $150 \mu\text{E m}^{-2} \text{s}^{-1}$.

yields in the absence of **1a**. Conversely, in the presence 10 mM **1a**, the WT and Δ Flv1 demonstrated lower Y(II) (Figure 5, with **1a**) under illumination, compared to the cells incubated without the substrate. Importantly, this Y(II) decrease was rescued by the introduction of YqjM to the WT and Δ Flv1 strains. Notably, Δ Flv1::P_{cpc}YqjM displayed a somewhat higher Y(II) compared to Syn::P_{cpc}YqjM. Compared to cells kept in preconditions without **1a**, the WT and Δ Flv1 exposed to the substrate had markedly higher Y(I) in far red light but a relatively unchanged yield in red light; while Syn::P_{cpc}YqjM and Δ Flv1::P_{cpc}YqjM had comparable Y(I) regardless of the presence or absence of **1a**. These results indicated that **1a** has adverse and toxic effects on the photosynthetic machinery, especially PSII, and that the introduction of YqjM mitigates these negative effects by rapidly converting intracellular **1a** to the product **1b**.

In order to translate these observations to cell viability and growth, viability assays in liquid cultures using 10, 25, 50, and 100 mM of **1a** and **1b** were conducted on Syn WT and Syn::P_{cpc}YqjM. In all tests, the product **1b** did not show toxicity as cells tolerated all tested concentrations; growing back on solid media even after 24 h of exposure (Figure 5c,d). As expected, **1a** was much more toxic; as evidenced by the lack of WT growth after exposure to concentrations over 25 mM for 30 min (Figure 5c). In contrast, recombinant cells could be recultivated, albeit in a reduced fashion, after exposure to concentrations >25 mM for a period of 1 h (Figure 5c). The tolerance of the recombinant Syn::P_{cpc}YqjM cells was also reflected by their activity, as complete conversions of 10 mM within 1 h, 25 mM within 4 h, and 50 mM within 7 h were

possible (SI, Figure S2). Viability assays using Syn::P_{psbA2}YqjM can be found in the Supporting Information (SI, Figure S5).

Disruption of the Flv1/Flv3 Electron Valve Enhances YqjM Activity. The kinetic parameters of the enzyme (Figure 3) show clearly that the reductive-step is the rate limiting step of the YqjM-catalyzed ene-reduction. Hence, we assumed that by removing competing electron sinks, more electrons may be funnelled toward YqjM, leading to accelerated reaction rates in the whole-cell biotransformations. Potential electron channeling toward heterologous YqjM was done through the use of Synechocystis mutants lacking Flv1 and Flv3 which are known to work as a heterodimer to protect PSI.^{34,45}

The activities of YqjM expressed in Flv1 and Flv3 deletion mutants were initially evaluated using cells, at a final OD₇₅₀ \sim 10, that were cultivated under standard cultivation conditions ($60 \mu\text{E m}^{-2} \text{s}^{-1}$, $30 \text{ }^\circ\text{C}$). Under those growth conditions, no significant differences in product formation rates and specific activities between Syn::P_{cpc}YqjM and Δ Flv1::P_{cpc}YqjM was observed (SI, Figure S6). We, therefore, speculated that effects—if any—would become apparent for cells cultured at higher light intensities due to the natural role of flavodiiron proteins, that are involved in photoprotection and acclimation.

The results presented (Figure 6) were obtained using cells cultivated at increased light intensities of $150 \mu\text{E m}^{-2} \text{s}^{-1}$ with the biotransformations themselves conducted in a photobioreactor⁴⁶ with light intensities within the same range.

We observed that the gene deletions, which prevent the formation of the Flv1/Flv3 heterodimer, led to improvements in the *in vivo* YqjM-mediated reduction of **1a** at final cell densities where significant self-shading is expected (OD750

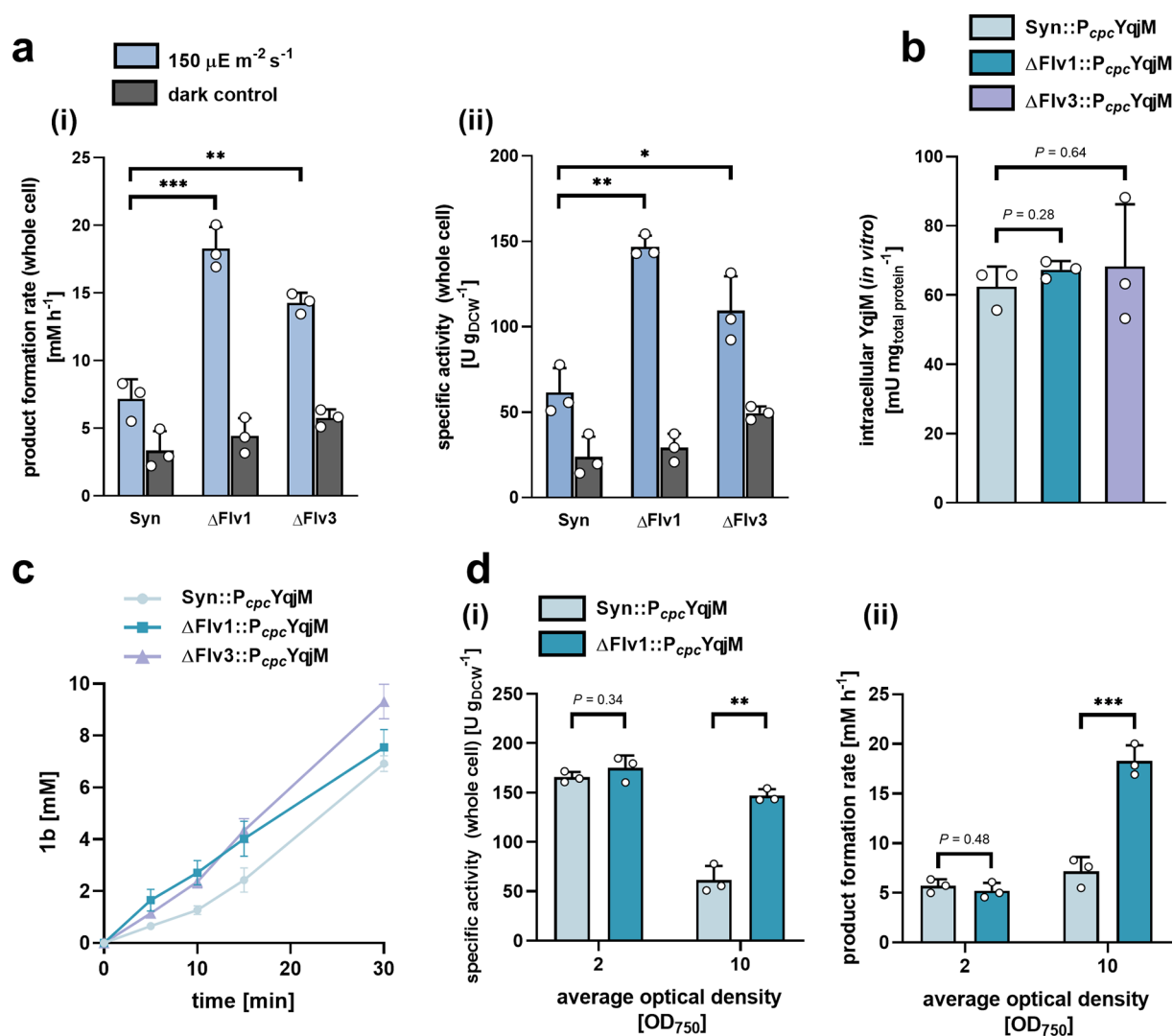


Figure 6. Comparison of [a (i)] product formation rate and [a (ii)] specific whole cell activity normalized to cell density of Syn::P_{cpc}YqjM and the corresponding deletion mutants, ΔFlv1::P_{cpc}YqjM and ΔFlv3::P_{cpc}YqjM, carried out at an OD₇₅₀ ~10. Panel [b] presents active intracellular YqjM concentrations (relative to total protein), determined *in vitro*, between the three strains expressing YqjM under control of the P_{cpc} promoter. [c] shows examples of product formation over time at an OD₇₅₀ ~ 10, the values within the first 5–10 min were used for calculations whenever relevant. The effects of reducing the cell density used for biotransformations on [d (i)] whole cell specific activities normalized to cell density and [d (ii)] product formation rate are shown for the strains Syn::P_{cpc}YqjM and ΔFlv1::P_{cpc}YqjM and is compared to the values derived at an OD₇₅₀ of 10. In all cases, the starting concentration of **1a** was ~10 mM. All bars represent data generated from reactions stemming from biological replicates (*N* = 3) with individual values depicted. Error bars represent SD. *P*-values were calculated using Welch's *t* test and represent comparisons between Syn::P_{cpc}YqjM and respective deletion mutant (****P* < 0.001, ***P* < 0.01, **P* < 0.05). Exact *P*-values where asterisks are placed can be found in the raw data files.

~10, chl_a = ~ 60 μg mL⁻¹). Specifically, the product formation rate of ΔFlv1::P_{cpc}YqjM and ΔFlv3::P_{cpc}YqjM resulted in a 2.70- and 2-fold improvement compared to Syn::P_{cpc}YqjM, respectively (Figure 6a (i)). This effect held true when activities were normalized to cell density (Figure 6a (ii)) and to the content of the pigment chl_a (SI, Figure S7).

In order to rule out differences in enzymatic expression being responsible for improved activity, we determined active intracellular YqjM concentrations in an NADPH assay after cell disruption (for more details, refer to the Materials and Methods). These tests confirmed that YqjM levels, relative to total protein, did not significantly differ between Syn::P_{cpc}YqjM and any of the Flv deletion mutants (Figure 6b); thus, effectively ruling out enzymatic expression differences as the cause of activity enhancement. The dark control reactions performed, however, indicate that sugars naturally present in

the strains fuel at least a part of the reaction, albeit not to completion. We also noted that this dark activity was slightly more pronounced in both ΔFlv mutants. This may be attributed to an increased oxidative glycolytic metabolism brought about by the deletions which have been previously reported to occur in both *Synechocystis*³⁹ and *Chlamydomonas reinhardtii*.⁴⁷

The formation of the product, **1b**, across the first 30 min of biotransformations is shown in Figure 6c. At a starting substrate concentration of 10 mM, all strains achieve full conversion within 1h; at higher concentrations, however, the enhanced ΔFlv1::P_{cpc}YqjM activity was more pronounced. Using ΔFlv1::P_{cpc}YqjM, 25 mM and 50 mM of **1a** were converted completely within 1.5 and 3.5 h, respectively (SI, Figure S8) while Syn::P_{cpc}YqjM required between 3 and 4 h

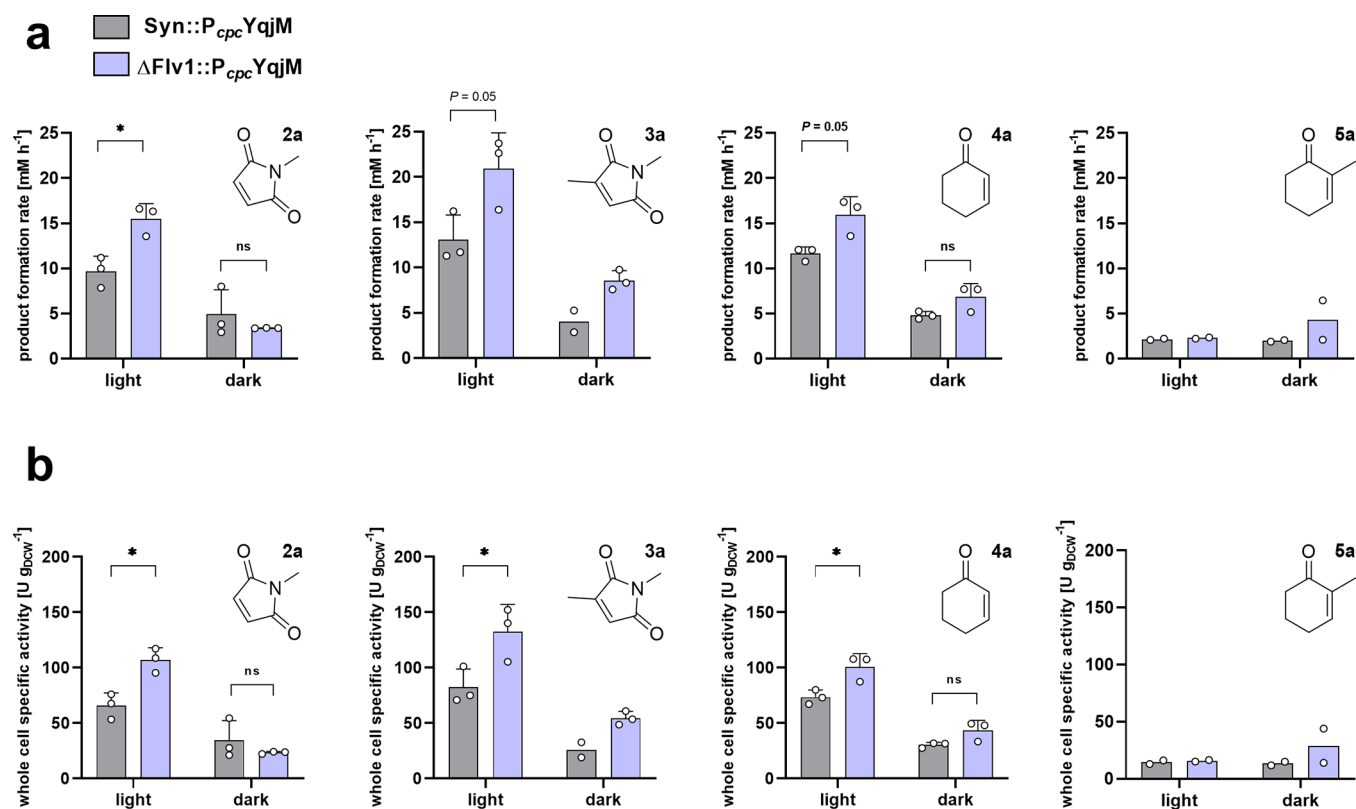


Figure 7. Evaluation of [a] product formation rate and [b] whole cell specific activity (normalized to dry cell weight) of YqjM using different substrates 2a–5a known to be accepted by YqjM using Syn::P_{cpc}YqjM and ΔFlv1::P_{cpc}YqjM. Biotransformations were carried out at an OD₇₅₀ ~ 10 and 10 mM substrate in a photobioreactor at an intensity of 150 μE m⁻² s⁻¹ and in the dark. All bars represent data generated from reactions stemming from biological replicates with individual values depicted. Error bars represent SD. P-values were calculated using Welch's *t* test or Mann–Whitney. (**P* < 0.05). Exact P-values where asterisks are placed can be found in the raw data files. (*N* = 2–3).

and 5–7 h to convert 25 and 50 mM, respectively (SI, Figure S2).

Next, we sought to investigate the effects of lowering the cell density at which biotransformations are conducted on the product formation rate and whole-cell specific activities using Syn::P_{cpc}YqjM and ΔFlv1::P_{cpc}YqjM. As foreseen, productivities are highest at low cell densities (OD₇₅₀ ~ 2) where less self-shading occurs (Figure 6d (i)). At moderate cell densities (OD₇₅₀ ~ 10), however, the productivity of Syn::P_{cpc}YqjM is negatively affected. This decrease in productivity appears to be indicative of NADPH limitations that arise due to light attenuation. Our results suggest that ΔFlv1::P_{cpc}YqjM may alleviate these limitations as evidenced by a 2-fold improvement in specific activity. This improvement translated into a remarkable increase of product formation rate from 7.2 mM h⁻¹ to 18.3 mM h⁻¹ (Figure 6d (ii)).

In order to demonstrate the effectiveness of the engineered cells for biocatalytic applications, we applied ΔFlv1::P_{cpc}YqjM at cell densities of 2.4 g_{DCW} L⁻¹ (OD₇₅₀ ~ 10) to convert higher concentrations of 1a to the product 1b. We noted that ΔFlv1::P_{cpc}YqjM could convert ~60 mM of substrate in 4 h and 83.4 mM in 6 h, representing conversions of 100% and 94%, respectively, when a substrate feeding approach was followed. Collectively, these results indicate that the deletion of competing NADPH-consuming pathways represents a feasible approach to improve heterologous redox reactions.

In order to further validate our results, we sought to try substrates other than 1a under the same conditions described. We noted that, indeed, the activity-enhancing effects we report

for ΔFlv1::P_{cpc}YqjM are only apparent for fast reactions where we assume NADPH limitation occurs. For the substrate 2-methylcyclohexenone (5a) almost no differences in reaction rates (~ 2 mM h⁻¹ and 15 U g_{DCW}⁻¹) under both dark and light conditions (Figure 7) were observed, and thus, the Flv-deletion mutant does not enhance the reaction. In contrast, the other substrates all had faster reaction rates with the ΔFlv1::P_{cpc}YqjM strain with a range of activities varying from 100 to 132 U g_{DCW}⁻¹. This shows that the rate-enhancing effect of the Flv-deletion applies for fast biotransformations. The fact that the conversion of 5a is not significantly accelerated indicates that here, the photosynthetic electron supply is sufficient to fuel this reaction.

DISCUSSION

Here we demonstrate that the combination of different engineering strategies like promoter engineering and the simultaneous deletion of electron sinks has the potential to overcome NADPH limitation in light-driven biocatalysis. Moreover, it is shown, for the first time, that determining *in vivo* NADPH fluorescence is a valuable tool when engineering light-fueled biotransformations in cyanobacteria.

The utilization of photoautotrophic cyanobacteria and other algal strains in biotechnology holds the potential to expand the repertoire of environmentally friendly industrial processes. However, various obstacles have to be overcome. It is clear that sufficient light availability is a critical factor for cyanobacterial growth⁴⁸ and for high productivity of NADPH-dependent heterologous reactions.⁴⁹ However, feasible catalytic applica-

tions of cyanobacteria would require cell densities higher than a few grams per liter to obtain industrially relevant space-time-yields. Under these conditions, the limited availability of light quickly turns into a major bottleneck; the production of photosynthetic reducing equivalents (e.g., NADPH) is compromised, thus leading to an insufficient electron supply for any fast whole-cell redox reaction. As such, various engineering approaches have been focused on genetic manipulation of cofactor metabolism to increase the availability of reducing equivalents.^{50,51}

In this work, the use of NADPH fluorescence for the characterization of a light-driven biotransformation with a recombinant NADPH dependent enzyme *in vivo* is shown. It has been previously applied to elucidate dynamic changes in intracellular NADPH levels and to demonstrate the interplay between light and dark reactions of cyanobacteria,⁵² the activity of the Calvin–Benson cycle upon decreasing inorganic carbon availability,⁵³ the induction of ferredoxin-NAD(P)H reductase (FNR) at dark-to-light transitions and relative *in vivo* NADPH pool size,⁴³ or to determine reaction partners of Flv1/Flv3.^{31,32} It is important to note that, although intracellular NADH may contribute to *in vivo* NADPH fluorescence, it is unlikely to be of significant value given that NADH concentrations are not expected to undergo dramatic light-dependent changes within the ms time-frames reported.^{43,52}

Using the model ene-reductase YqjM, we show that the implementation of a strong heterologous electron sink together with elimination of a natural electron outlet can significantly improve photosynthesis-driven bioproduction processes. The integration of YqjM in *Synechocystis* can be used to quantify additional NADPH consumption by substrate depletion and product formation.¹¹ With a specific activity of 680 $\mu\text{mol mg}_{\text{chla}}^{-1} \text{h}^{-1}$ ($\text{OD}_{750} \sim 2$, $\text{chla} \sim 6 \mu\text{g mL}^{-1}$) *Syn::P_{cpc}YqjM* constitutes a relatively strong and tunable electron sink that deviates at least $\sim 60\%$ of photosynthetically produced NADPH. This is based on Kauny and Sétif's estimation that the NADPH pool in *Synechocystis* has a photoproduction rate of 530–1079 $\mu\text{mol mg}_{\text{chla}}^{-1} \text{h}^{-1}$ (determined at a density equaling 2.5 $\mu\text{g mL}^{-1}$ *chla*).⁴³

We believe that the main reaction highlighted in this work, the stereoselective reduction of the substrate **1a**, is not only a model for highly selective biotransformations but may also be applied to probe NADPH in photoautotrophs to study other pathways that deviate a large percentage of photosynthetic reducing equivalents. This approach could even be partnered with existing screening technologies, such as CRISPRi-based screenings.⁵⁴

Other reported rates for recombinant whole-cell biotransformations in *Synechocystis* using heterologously produced oxidoreductases range from 5.5 $\text{U g}_{\text{DCW}}^{-1}$ for the monooxygenase AlkBGT,⁵⁵ 5.7 $\text{U g}_{\text{DCW}}^{-1}$ for the monooxygenase CHMO,²⁵ 20 $\text{U g}_{\text{DCW}}^{-1}$ for an imine reductase²³ to 39 $\text{U g}_{\text{DCW}}^{-1}$ for a P450 monooxygenase.¹³ In comparison, the YqjM rates we report are consistently higher than 50 $\text{U g}_{\text{DCW}}^{-1}$. We assume that activities beyond this would inflict severe NADPH-supply limitations and would, therefore, be a general problem for the acceleration of light-driven whole cell biotransformations. In order to alleviate some of this limitation, we sought to increase the NADPH available for enzymatic redox reactions by the deletion of the Flv1/Flv3 oligomer. By following this approach, we were able to successfully increase the specific activity of the ene-reduction of **1a** to $\sim 150 \text{ U g}_{\text{DCW}}^{-1}$ or 300 $\mu\text{mol mg}_{(\text{Chl})}^{-1} \text{h}^{-1}$ at a cell

density of 2.4 $\text{g}_{\text{DCW}} \text{L}^{-1}$ ($\text{OD}_{750} \sim 10$) where self-shading reduces light availability and causes light fluctuations within the vessel. This is key to consider as most bioreactors often experience light and dark zones^{56,57} and the optimization of photoautotrophs within these constraints can be industrially and economically relevant. In fact, the improved activity we reported at 2.4 $\text{g}_{\text{DCW}} \text{L}^{-1}$, does fall in line with the supposed role of the Flv1/Flv3 oligomer as a strong electron sink under fluctuating light.³⁴ It must be noted, however, that the ΔFlv mutants may be more light sensitive under specific conditions.^{31,58} Nonetheless, engineering heterologous strong electron sinks (e.g., YqjM) should overcome the imbalance between energy input and electron outlet eliminating oxidative stress and feedback reactions.

The product formation rate and specific activities we report with $\Delta\text{Flv1}::\text{P}_{\text{cpc}}\text{YqjM}$, represent, to our knowledge, the fastest overall rates reported for a light-powered biotransformation. Additionally, we assume that FDPs represent a significant source of NADPH oxidation⁵⁹ and, as a result, their removal would favor a higher YqjM activity. Nonetheless, the product formation rate of 18.3 mM h^{-1} that we report of at an optical density of 10 compares favorably to rates obtained by using hydrogen¹⁶ or catalytic water-oxidation *in vitro* as electron source.¹⁷

We would like to note that although the deletion of either Flv1 or Flv3 as a competing electron sink seemingly confirms the limiting role of NADPH availability for the biotransformation, their physiological effects may be more complex. The exact redox partner of Flv1/Flv3, for instance, is as of yet not fully elucidated. Recently, the work from two different laboratories^{31,32} identified Fd as the electron donor of FDPs in an *in vivo* study. However, other recent *in vitro* findings by Brown et al.²⁹ show that both Flv1 and Flv3 homodimers exhibit binding with NAD(P)H to catalyze the protective oxygen reduction reaction with efficiencies of $10^5 \text{ M}^{-1} \text{ s}^{-1}$.

In conclusion, our findings confirm that the supply of reduced redox cofactors for light-driven biotransformations in cyanobacteria is a limiting factor for the production of chemicals. This is further exacerbated by the reduction in photosynthetic activity due to lower light availability and fluctuating light, respectively, that cannot be avoided at higher cell densities. Nevertheless, the removal of natural electron sinks such as FDPs that are dispensable under controlled cultivation conditions appears to be a highly promising strategy to alleviate the effects of “self-shading”, which will be crucial for development of light-driven catalysts that can compete with current, cosubstrate-dependent systems.

■ MATERIALS AND METHODS

Chemicals and Reagents. The substrate, 2-methylmaleimide (**1a**), and its product, 2-methylsuccinimide (**1b**) were obtained as white powder from the manufacturer Chiracon GmbH (Luckenwalde, Germany). All other materials were purchased from Sigma-Aldrich (Steinheim, Germany) or Carl Roth (Karlsruhe, Germany) unless otherwise indicated.

Strains and Plasmid. A list of all strains and plasmids used in this study is given in Table S1.

Plasmid Construction. FastCloning was used to clone the integrative plasmids *SynRekB_P_{cpc}YqjM* and *SynRekB_P_{zia}YqjM*. The genome of *Synechocystis* was isolated and used as the template to amplify the sequences for the promoters and their upstream regions. 628 bp upstream to the *cpcB* gene were amplified for the *P_{cpc}* promoter as previously

reported. The cloned sequence for the P_{zia} promoter includes the repressor gene *ziaR*. The primers used for the cloning of these vectors are given in Table S2.

Construction of Synechocystis Mutants. All transformed strains in this work were generated by homologous recombination using plasmids described in Table S1, targeting the gene locus *slr0168*. WT and mutant strains were cultured at 30 °C in liquid BG-11 medium (pH = 8) and in an atmosphere of 50% humidity and atmospheric CO₂ levels. Cultures were agitated by a rotary shaker at 140 rpm under white fluorescent light (60 $\mu\text{E m}^{-2} \text{s}^{-1}$). Cells were grown to their midexponential phase (OD₇₅₀ 0.5–1) and washed with fresh BG-11, and subsequent natural transformation was carried out by mixing plasmid DNA (2–5 μg) with cells in a sterile tube (1.5 mL). This mixture was shaken in darkness (140 rpm) for a period of 5 h after which cells were plated on a sterile nitrocellulose membrane (GE Healthcare, catalog number: 11314874) placed on antibiotic free BG-11 plates. After 24 h, the membrane was transferred to a plate with low concentrations of the required antibiotics (10–25 $\mu\text{g mL}^{-1}$) until colonies were discernible (10–21 days). As *Synechocystis* is polyploid in nature, complete segregation of the mutant alleles was achieved by restreaking the colonies onto plates supplemented with gradually increasing levels of antibiotics (50–150 $\mu\text{g mL}^{-1}$). Segregation was confirmed via colony PCR. The used primers are listed in SI, Table S2.

Standard Cultivation and Maintenance Conditions. Seed cultures in liquid and on plates were maintained in a plant growth chamber (SWGC-1000, WISD lab instruments) under atmospheric carbon dioxide conditions, fitted with white fluorescent lamps that provide 24 h illumination at an average intensity falling within 40–60 $\mu\text{E m}^{-2} \text{s}^{-1}$. The chamber was set to a temperature of 30 °C and humidity levels of 50%. Cells were cultured in 50, 100, or 300 mL Erlenmeyer flasks (working volumes: 25, 50, and 100 mL, respectively) on rotary shakers fitted within the chamber (140 rpm). Kanamycin (50 $\mu\text{g/mL}$) was used as selective antibiotic for all strains containing an expression cassette for YqjM. Additionally, ΔFlv1 and ΔFlv3 variants were supplemented with chloramphenicol (10 $\mu\text{g/mL}$) or spectinomycin (30 $\mu\text{g/mL}$), respectively.

Higher Light Cultivation Conditions. *Synechocystis* was cultivated in Erlenmeyer flasks (300 mL, working volume: 100 mL) in standard BG-11 containing the respective antibiotics at room temperature. Cultures were agitated on a rotary shaker (140 rpm) and illuminated following a constant light regime by a tunable LED lamp (CellDEG, Berlin, Germany) emitting mostly blue and red light (intensity of $\sim 150 \mu\text{E m}^{-2} \text{s}^{-1}$), spectra can be found in the SI (Figure S9). Cultures were grown until they reached an OD₇₅₀ of 2–2.5, which typically required between 6–7 days. A graphical depiction of this particular set up is shown in the SI (Figure S10).

The light intensity was measured with a LI-250A light meter (LICOR Biosciences, Hamburg, Germany) and a submersible spherical micro quantum sensor, US-SQS/L (Walz, Effeltrich, Germany). A graphical depiction of light intensity measurement using both sensors and a table showing the values is shown in the SI (Figure S11, Table S3).

Quantification of Chlorophyll *a* Content. The content of *chl_a* was determined using methanol extraction as described previously. This was done for all strains discussed in this work and was used to generate line graphs to determine the relationship between the total *chl_a* content and the

corresponding optical density (OD₇₅₀). These graphs are presented in the SI (Figure S12).

Quantification of the Dry Cell Weight. Cells were grown to an OD₇₅₀ of 2–2.5 and harvested by centrifugation. The cell pellet was resuspended in BG-11 medium to yield different optical densities. Samples from these (1 mL) were centrifuged, and the pellets were washed twice with Milli Q water before being dried in an incubator (60 °C). The resulting dried cell mass was weighed, and corresponding values were plotted against its respective OD₇₅₀. A line graph depicting this is provided in the SI (Figure S13).

Light-Driven Biotransformations. After cultivation at standard or higher light conditions, cells were harvested by centrifugation (24 °C, 25 min, 3220g) and the resulting pellet was resuspended in fresh BG-11 to reach the desired optical density (measured at 750 nm). Whole-cell biotransformations were performed at 30 °C in 5 mL glass vials (working volume 1 mL) and were started by the addition of **1a–5a** in the respective concentration. The vials were placed into a bioreactor equipped with LED lamps (average intensity 150 $\mu\text{E m}^{-2} \text{s}^{-1}$) and were agitated (140 rpm). Multiple samples were taken as required at different time-points and typically included samples at the start (t₀) and after 5, 10, 15, 30, 60, and 120 min with further sampling if necessary. The samples were directly frozen in liquid nitrogen to quench the reaction. Relevant control reactions were conducted in BG-11, under dark conditions and with WT cells—these are shown in the SI (Figures S14, S15). All substrate and product stocks **1b** were prepared in BG-11.

Cell Disruption. Cells (1 mL, OD₇₅₀ ≈ 20) were centrifuged (3 min, 4 °C, 16 000g), and the pellet was washed by resuspending it in PBS (137 mM NaCl, 2.7 mM KCl, 10 mM Na₂HPO₄, 1.8 mM KH₂PO₄, pH = 7.4, 2 mL). After subsequent centrifugation (5 min, 4 °C, 16 000g), the supernatant was discarded, and the cells were resuspended in PBS (200 μL). The proteinase inhibitor aminocaproic acid (1 mM) and glass beads (diameter 0.25 mm) were added. Subsequently, cells were disrupted by vortexing (4 times x 30 s) with cooling breaks on ice (2 min) in between. After centrifugation (5 min, 4 °C, 16 000g), PBS (100 μL) was added, and the resulting blue colored cell lysate was carefully separated from the glass beads. The protein concentration of the crude cell extract was determined with BCA assay (ThermoFisher Scientific, catalog number: 23227) using BSA solution (25–2000 $\mu\text{g/mL}$) as a standard for calibration. Cell lysate was used for the *in vitro* NADPH assay and SDS-PAGE analysis.

In Vitro NAD(P)H Assay. Potassium buffer (20 mM, pH = 6.5) was degassed by sparging with N₂ for 10 min. **1a** (1 mM) and NAD(P)H (125 μM) were mixed with buffer in a cuvette. The reaction was started by the addition of cell lysate (100 μL) and the absorption at 340 nm was monitored for 3 min. An example of the raw data generated is given in the SI along with the determination of the respective extinction coefficients (SI, Figures S16, S17). Control reactions without the addition of substrates were performed for every lysate sample to subtract background reactions. The activity in $\text{mU mg}_{\text{total protein}}^{-1}$ was then calculated from the slope and extinction coefficient for NAD(P)H, and the protein concentrations determined with the BCA assay.

Viability Assay. Toxicity effects of **1a** and **1b** were investigated in the relevant time span for biotransformations as described previously. Substrate and product were added at final

concentrations of 10, 25, 50, and 100 mM. To the respective time points, samples (100 μL) were taken and washed twice with BG-11 (500 μL). Cells were pelleted by centrifugation and streaked with a toothpick.

Quantitative GC-FID Analysis. GC-FID (GC-2010 Plus, Shimadzu, Japan) equipped with a ZB-5 column was used to analyze samples taken from biotransformations of **1a–4a**. **5a** and **5b** were analyzed on GC-FID (GC-2030, Shimadzu, Japan) equipped with a hydrodex β -TBDAC column. Sample preparation was carried out by organic phase extraction using ethyl-acetate for compounds **1–5**. 1-Decanol (2 mM) was used as an internal standard. Detailed description of the utilized separation method is available in the SI (Table S4). Additionally, a sample chromatogram and calibration for the substrate (**1a**) and product (**1b**) can be found (SI, Figure S18, S19).

In Vivo NADPH Decay Measurements. NADPH fluorescence measurements were performed using the NADPH/9-AA module of a DUAL-PAM 100 device (Walz, Germany) following the general set up and software settings described in the work of Kauny and Sétif. Samples for measurements were prepared by growing cultures (50 mL) until an OD₇₅₀ of 1 was reached (30 °C, light intensity: 50 $\mu\text{E m}^{-2} \text{s}^{-1}$). Cultures (20 mL) were harvested by centrifugation (4000g, 10 min, room temperature) and the sedimented cells were washed once with fresh BG-11 medium then resuspended to reach the final chlorophyll *a* concentration (2.5 $\mu\text{g mL}^{-1}$). Then, cells were incubated at growth conditions for 30 min prior to the measurements. For measurements, cells from each culture (3 mL) were preincubated in a quartz cuvette at 30 °C under actinic light (AL) with an intensity of $\sim 120 \mu\text{E m}^{-2} \text{s}^{-1}$ and were alternated with dark periods using a regimen of 30 s on, 10 s off. Directly afterward, FastKinetics were measured using a 20 s Clock interval starting a trigger run that was as follows: AL off with a delay of 100 ms, AL on at 3000 ms, AL stays on after each triggered run. NADPH ML frequency was 5000 Hz during illumination and 100 Hz in darkness. A total of 20 measurements were averaged to obtain a sufficient signal-to-noise ratio. Samples were measured with or without the addition **1a** (30 μL , 100 mM, final concentration 1 mM). If substrate was added, cells were mixed by pipetting and incubated under illumination (20 s) before starting the measurement. Data was normalized to 0 at the end of dark incubation. Steady-state fluorescence during illumination was determined by averaging the signal within the -100 ms delay in the beginning. The NADPH decay rate constant [b] was determined by fitting the decay part of the curves in the SigmaPlot software using the function: $f = y_0 + a - b * x$.

Determination of Photosynthetic Parameters. Chlorophyll fluorescence and P700 redox kinetics in intact cells were determined by a pulse amplitude-modulated fluorometer (Dual-PAM-100, Walz, Germany). Prior to the activity measurements, chlorophyll *a* concentration was adjusted to 15 $\mu\text{g mL}^{-1}$, and cells were exposed to 400 $\mu\text{E m}^{-2} \text{s}^{-1}$ white light in AlgaeTRON AG130 cool-white LED chambers (PSI Instruments, Czech Republic) for 15 min (in the presence or absence of 10 mM **1a**). Then, the sample cells were transferred to the sample holder of the instrument and kept in darkness for 1–2 min. During the measurements, multiple turnover saturating pulses (5000 $\mu\text{E m}^{-2} \text{s}^{-1}$, 500 ms) were applied under far red (720 nm, 40 W m^{-2}) and actinic red (635 nm, 50 $\mu\text{E m}^{-2} \text{s}^{-1}$) illumination. Yields of PSI and PSII were calculated as described previously.^{60,61}

Determination of YqjM Kinetic Parameters. In order to determine the reductive rate of YqjM, the rate of cofactor reduction was determined in an anaerobic glovebox using a stopped flow device equipped with a photomultiplier. Prior to the measurements, samples were flushed with nitrogen and incubated in the glovebox. A final concentration of 25 μM YqjM was shot against 30–1000 μM of NADPH or NADH using Tris-HCl (50 mM, pH 7.5) as a reaction buffer and the rapid reactions were recorded at 452 nm at 25 °C. The observed rates of cofactor reduction were plotted against the final concentration of NADPH or NADH to determine k_{red} and K_{D} .

The oxidative rate of YqjM was determined by the same device, anaerobic conditions were achieved as described above. For this experiment, the enzyme was reduced by adding approximately equimolar amounts of NADPH to the YqjM solution until approximately a 90% reduced flavin spectrum was observed. This reduced protein sample (final concentration: 20 μM YqjM) was then shot against a solution of **1a** in buffer (final concentration of 25–500 μM) and the rapid reactions were recorded at 452 nm at 25 °C in Tris-HCl (50 mM, pH 7.5). In this setup, no saturation was observed, because the reaction progressed too rapidly to be measured at high substrate concentrations; therefore, only the biomolecular rate k_{ox} of $2.08 \pm 0.02 * 10^6 \text{ M}^{-1} \text{ s}^{-1}$ was determined.

Steady-state kinetics (SI, Figure S3) were determined by following the oxidation of 100 μM NADPH at 340 nm in Tris-HCl (50 mM, pH 7.5) at 25 °C using 100 nm of YqjM and 25–5000 μM **1a**. Stock solutions of **1a** were prepared in the assay buffer.

Statistical Analysis of Experimental Data. Unless otherwise indicated, statistical testing was performed using the appropriate tools in GraphPad Prism version 8.0. Unpaired Welch's *t* test or Mann–Whitney was utilized for the analysis of two groups where data followed Gaussian distribution or violated it, respectively. The assumption of normality was assessed using Shapiro–Wilk's test. For comparisons including three groups, one-way analysis of variance (ANOVA) was used, and the following pairwise comparisons were carried out using Tukey's posthoc. The samples which were chosen for analysis were derived from a minimum of three independent experiments and cultivations. Data are presented as bar-graphs, line-graphs or in-text showing the mean \pm SD as indicated. Wherever applicable, significance reported is based on an alpha value of 0.05 and is always two-sided.

■ ASSOCIATED CONTENT

Supporting Information

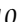
The Supporting Information is available free of charge at <https://pubs.acs.org/doi/10.1021/acscatal.0c02601>.

Information about strains and plasmids, light spectra, analytics, and additional data and figures mentioned in the manuscript (PDF)

Relevant raw data and statistics of results shown (XLSX)

■ AUTHOR INFORMATION

Corresponding Authors

Robert Kourist – Institute of Molecular Biotechnology, Graz University of Technology, 8010 Graz, Austria;  orcid.org/0000-0002-2853-3525; Email: kourist@tugraz.at

Marc M. Nowaczyk – Department of Plant Biochemistry, Faculty of Biology & Biotechnology, Ruhr University Bochum, 44780 Bochum, Germany; Email: marc.m.nowaczyk@rub.de

Authors

Leen Assil-Companioni – Institute of Molecular Biotechnology, Graz University of Technology, 8010 Graz, Austria; ACIB GmbH, 8010 Graz, Austria

Hanna C. Büchschütz – Institute of Molecular Biotechnology, Graz University of Technology, 8010 Graz, Austria

Dániel Solymosi – Molecular Plant Biology unit, Department of Biochemistry, Faculty of Science and Engineering, University of Turku, Turku 20014, Finland

Nina G. Dyczmons-Nowaczyk – Department of Plant Biochemistry, Faculty of Biology & Biotechnology, Ruhr University Bochum, 44780 Bochum, Germany

Kristin K. F. Bauer – Institute of Molecular Biotechnology, Graz University of Technology, 8010 Graz, Austria

Silvia Wallner – Institute of Biochemistry, Graz University of Technology, 8010 Graz, Austria

Peter Macheroux – Institute of Biochemistry, Graz University of Technology, 8010 Graz, Austria

Yagut Allahverdiyeva – Molecular Plant Biology unit, Department of Biochemistry, Faculty of Science and Engineering, University of Turku, Turku 20014, Finland

Complete contact information is available at:
<https://pubs.acs.org/10.1021/acscatal.0c02601>

Author Contributions

*L.A.-C. and H.C.B. contributed equally to this work

Author Contributions

R.K. and M.M.N. conceived the project and main conceptual ideas. L.A.-C. and H.C.B. equally contributed to the development of the project, performed measurements, analyzed results, drafted the manuscript and designed figures. D.S. performed photosynthetic activity experiments, N.G.D.-N. performed NADPH decay measurements, K.K.F.B. contributed to YqjM activity measurements under standard conditions and S.W. determined the kinetics of YqjM experimentally. P.M. supervised YqjM kinetics experiments and Y.A. supervised photosynthetic activity experiments and provided valuable insights. All authors discussed results, contributed to the writing of the manuscript and provided critical commentary.

Notes

The authors declare no competing financial interest.

ACKNOWLEDGMENTS

The authors thank the Austrian Science Funds (FWF, P31001-B29), Deutsche Bundesstiftung Umwelt (DBU, AZ 33741/01-32) and the NordForsk Nordic Center of Excellence “NordAqua” (#82845) for financial support. We also thank Chiracon GmbH for the synthesis and provision of key compounds used in this study. Furthermore, we thank Dr. Elia Calderini (TU Graz) and Dr. Dmytro Neshchadin (TU Graz) for support and measurements of light spectra.

REFERENCES

- (1) Claessens, N. J.; Sousa, D. Z.; dos Santos, V. A. P. M.; de Vos, W. M.; van der Oost, J. Harnessing the Power of Microbial Autotrophy. *Nat. Rev. Microbiol.* **2016**, *14* (11), 692–706.
- (2) Janssen, P. J. D.; Lambreva, M. D.; Plumeré, N.; Bartolucci, C.; Antonacci, A.; Buonasera, K.; Frese, R. N.; Scognamiglio, V.; Rea, G.

Photosynthesis at the Forefront of a Sustainable Life. *Front. Chem.* **2014**, *2* (36). DOI: 10.3389/fchem.2014.00036

(3) Maeda, Y.; Yoshino, T.; Matsunaga, T.; Matsumoto, M.; Tanaka, T. Marine Microalgae for Production of Biofuels and Chemicals. *Curr. Opin. Biotechnol.* **2018**, *50*, 111–120.

(4) Chew, K. W.; Yap, J. Y.; Show, P. L.; Suan, N. H.; Juan, J. C.; Ling, T. C.; Lee, D.-J.; Chang, J.-S. Microalgae Biorefinery: High Value Products Perspectives. *Bioresour. Technol.* **2017**, *229*, 53–62.

(5) Yarnold, J.; Karan, H.; Oey, M.; Hankamer, B. Microalgal Aquafeeds as Part of a Circular Bioeconomy. *Trends Plant Sci.* **2019**, *24* (10), 959–970.

(6) Lauenstein, K. J.; Baier, T.; Wichmann, J.; Würdenweber, R.; Mussnug, J. H.; Hübner, W.; Huser, T.; Kruse, O. Efficient Phototrophic Production of a High-Value Sesquiterpenoid from the Eukaryotic Microalga *Chlamydomonas reinhardtii*. *Metab. Eng.* **2016**, *38*, 331–343.

(7) Liu, X.; Miao, R.; Lindberg, P.; Lindblad, P. Modular Engineering for Efficient Photosynthetic Biosynthesis of 1-Butanol from CO₂ in Cyanobacteria. *Energy Environ. Sci.* **2019**, *12* (9), 2765–2777.

(8) Chin, T.; Okuda, Y.; Ikeuchi, M. Sorbitol Production and Optimization of Photosynthetic Supply in the Cyanobacterium *Synechocystis* PCC 6803. *J. Biotechnol.* **2018**, *276–277*, 25–33.

(9) Knoot, C. J.; Ungerer, J.; Wangikar, P. P.; Pakrasi, H. B. Cyanobacteria: Promising Biocatalysts for Sustainable Chemical Production. *J. Biol. Chem.* **2018**, *293* (14), 5044–5052.

(10) Kirsch, F.; Luo, Q.; Lu, X.; Hagemann, M. Inactivation of Invertase Enhances Sucrose Production in the Cyanobacterium *Synechocystis* sp. PCC 6803. *Microbiology* **2018**, *164* (10), 1220–1228.

(11) Köninger, K.; Gómez Baraibar, Á.; Mügge, C.; Paul, C. E.; Hollmann, F.; Nowaczyk, M. M.; Kourist, R. Recombinant Cyanobacteria for the Asymmetric Reduction of C = C Bonds Fueled by the Biocatalytic Oxidation of Water. *Angew. Chem., Int. Ed.* **2016**, *55* (18), 5582–5585.

(12) Hoschek, A.; Schmid, A.; Bühler, B. *In Situ* O₂ Generation for Biocatalytic Oxyfunctionalization Reactions. *ChemCatChem* **2018**, *10* (23), 5366–5371.

(13) Hoschek, A.; Toepel, J.; Hochkeppel, A.; Karande, R.; Bühler, B.; Schmid, A. Light-dependent and Aeration-independent Gram-scale Hydroxylation of Cyclohexane to Cyclohexanol by CYP450 Harboring *Synechocystis* sp. PCC 6803. *Biotechnol. J.* **2019**, *14* (8), No. 1800724.

(14) Wen, X.; Du, K.; Wang, Z.; Peng, X.; Luo, L.; Tao, H.; Xu, Y.; Zhang, D.; Geng, Y.; Li, Y. Effective Cultivation of Microalgae for Biofuel Production: A Pilot-Scale Evaluation of a Novel Oleaginous Microalga *Graesiella* sp. WBG-1. *Biotechnol. Biofuels* **2016**, *9*, 123.

(15) Hubble, D. S.; Harper, D. M. Impact of Light Regimen and Self-Shading by Algal Cells on Primary Productivity in the Water Column of a Shallow Tropical Lake (Lake Naivasha, Kenya). *Lakes Reservoirs* **2001**, *6* (2), 143–150.

(16) Lauterbach, L.; Lenz, O.; Vincent, K. A. H₂-Driven Cofactor Regeneration with NAD(P)⁺-Reducing Hydrogenases. *FEBS J.* **2013**, *280* (13), 3058–3068.

(17) Kuk, S. K.; Singh, R. K.; Nam, D. H.; Singh, R.; Lee, J.-K.; Park, C. B. Photoelectrochemical Reduction of Carbon Dioxide to Methanol through a Highly Efficient Enzyme Cascade. *Angew. Chem., Int. Ed.* **2017**, *56* (14), 3827–3832.

(18) Nakamura, K.; Yamanaka, R. Light Mediated Cofactor Recycling System in Biocatalytic Asymmetric Reduction of Ketone. *Chem. Commun.* **2002**, No. 16, 1782–1783.

(19) Nakamura, K.; Yamanaka, R. Light-Mediated Regulation of Asymmetric Reduction of Ketones by a Cyanobacterium. *Tetrahedron: Asymmetry* **2002**, *13* (23), 2529–2533.

(20) Hölsch, K.; Havel, J.; Haslbeck, M.; Weuster-Botz, D. Identification, Cloning, and Characterization of a Novel Ketoreductase from the Cyanobacterium *Synechococcus* sp. Strain PCC 7942. *Appl. Environ. Microbiol.* **2008**, *74* (21), 6697–6702.

- (21) Pesic, M.; Fernández-Fueyo, E.; Hollmann, F. Characterization of the Old Yellow Enzyme Homolog from *Bacillus Subtilis* (YqjM). *ChemistrySelect* **2017**, *2* (13), 3866–3871.
- (22) Kitzing, K.; Fitzpatrick, T. B.; Wilken, C.; Sawa, J.; Bourenkov, G. P.; Macheroux, P.; Clausen, T. The 1.3 Å Crystal Structure of the Flavoprotein YqjM Reveals a Novel Class of Old Yellow Enzymes. *J. Biol. Chem.* **2005**, *280* (30), 27904–27913.
- (23) Büchsenschütz, H. C.; Vidimce-Risteski, V.; Eggbauer, B.; Schmidt, S.; Winkler, C. K.; Schrittwieser, J. H.; Kroutil, W.; Kourist, R. Stereoselective Biotransformations of Cyclic Imines in Recombinant Cells of *Synechocystis* Sp. PCC 6803. *ChemCatChem* **2020**, *12* (3), 726–730.
- (24) Sengupta, A.; Sunder, A. V.; Sohoni, S. V.; Wangikar, P. P. The Effect of CO₂ in Enhancing Photosynthetic Cofactor Recycling for Alcohol Dehydrogenase Mediated Chiral Synthesis in Cyanobacteria. *J. Biotechnol.* **2019**, *289*, 1–6.
- (25) Böhmer, S.; Königer, K.; Gómez-Baraibar, Á.; Bojarra, S.; Mügge, C.; Schmidt, S.; Nowaczyk, M.; Kourist, R. Enzymatic Oxyfunctionalization Driven by Photosynthetic Water-Splitting in the Cyanobacterium *Synechocystis* sp. PCC 6803. *Catalysts* **2017**, *7* (8), 240.
- (26) Esteves-Ferreira, A. A.; Inaba, M.; Fort, A.; Araújo, W. L.; Sulpice, R. Nitrogen Metabolism in Cyanobacteria: Metabolic and Molecular Control, Growth Consequences and Biotechnological Applications. *Crit. Rev. Microbiol.* **2018**, *44* (5), 541–560.
- (27) Zhang, C.-C.; Zhou, C.-Z.; Burnap, R. L.; Peng, L. Carbon/Nitrogen Metabolic Balance: Lessons from Cyanobacteria. *Trends Plant Sci.* **2018**, *23* (12), 1116–1130.
- (28) Vicente, J. B.; Gomes, C. M.; Wasserfallen, A.; Teixeira, M. Module Fusion in an A-Type Flavoprotein from the Cyanobacterium *Synechocystis* Condenses a Multiple-Component Pathway in a Single Polypeptide Chain. *Biochem. Biophys. Res. Commun.* **2002**, *294* (1), 82–87.
- (29) Brown, K. A.; Guo, Z.; Tokmina-Lukaszewska, M.; Scott, L. W.; Lubner, C. E.; Smolinski, S.; Mulder, D. W.; Bothner, B.; King, P. W. The Oxygen Reduction Reaction Catalyzed by *Synechocystis* sp. PCC 6803 Flavodiiron Proteins. *Sustain. Energy Fuels* **2019**, *3* (11), 3191–3200.
- (30) Santana-Sanchez, A.; Solymosi, D.; Mustila, H.; Bersanini, L.; Aro, E.-M.; Allahverdiyeva, Y. Flavodiiron Proteins 1–to-4 Function in Versatile Combinations in O₂ Photoreduction in Cyanobacteria. *eLife* **2019**, *8*, No. e45766.
- (31) Nikkanen, L.; Santana Sánchez, A.; Ermakova, M.; Rögner, M.; Cournac, L.; Allahverdiyeva, Y. Functional Redundancy between Flavodiiron Proteins and NDH-1 in *Synechocystis* sp. PCC 6803. *Plant J.* **2020**, *103*, 1460–1476.
- (32) Sétif, P.; Shimakawa, G.; Krieger-Liszakay, A.; Miyake, C. Identification of the Electron Donor to Flavodiiron Proteins in *Synechocystis* sp. PCC 6803 by *in Vivo* Spectroscopy. *Biochim. Biophys. Acta, Bioenerg.* **2020**, *1861* (10), 148256.
- (33) Helman, Y.; Tchernov, D.; Reinhold, L.; Shibata, M.; Ogawa, T.; Schwarz, R.; Ohad, I.; Kaplan, A. Genes Encoding A-Type Flavoproteins Are Essential for Photoreduction of O₂ in Cyanobacteria. *Curr. Biol.* **2003**, *13* (3), 230–235.
- (34) Allahverdiyeva, Y.; Mustila, H.; Ermakova, M.; Bersanini, L.; Richaud, P.; Ajlani, G.; Battchikova, N.; Cournac, L.; Aro, E.-M. Flavodiiron Proteins Flv1 and Flv3 Enable Cyanobacterial Growth and Photosynthesis under Fluctuating Light. *Proc. Natl. Acad. Sci. U. S. A.* **2013**, *110* (10), 4111–4116.
- (35) Jokel, M.; Johnson, X.; Peltier, G.; Aro, E.-M.; Allahverdiyeva, Y. Hunting the Main Player Enabling *Chlamydomonas reinhardtii* Growth under Fluctuating Light. *Plant J.* **2018**, *94* (5), 822–835.
- (36) Helman, Y.; Barkan, E.; Eisenstadt, D.; Luz, B.; Kaplan, A. Fractionation of the Three Stable Oxygen Isotopes by Oxygen-Producing and Oxygen-Consuming Reactions in Photosynthetic Organisms. *Plant Physiol.* **2005**, *138* (4), 2292–2298.
- (37) Allahverdiyeva, Y.; Ermakova, M.; Eisenhut, M.; Zhang, P.; Richaud, P.; Hagemann, M.; Cournac, L.; Aro, E.-M. Interplay between Flavodiiron Proteins and Photorespiration in *Synechocystis* sp. PCC 6803. *J. Biol. Chem.* **2011**, *286* (27), 24007–24014.
- (38) Berepiki, A.; Gittins, J. R.; Moore, C. M.; Bibby, T. S. Rational Engineering of Photosynthetic Electron Flux Enhances Light-Powered Cytochrome P450 Activity. *Synth. Biol.* **2018**, *3* (1), ysy009.
- (39) Thiel, K.; Patrikainen, P.; Nagy, C.; Fitzpatrick, D.; Pope, N.; Aro, E.-M.; Kallio, P. Redirecting Photosynthetic Electron Flux in the Cyanobacterium *Synechocystis* sp. PCC 6803 by the Deletion of Flavodiiron Protein Flv3. *Microb. Cell Fact.* **2019**, *18* (1), 189.
- (40) Jokel, M.; Nagy, V.; Tóth, S. Z.; Kosourov, S.; Allahverdiyeva, Y. Elimination of the Flavodiiron Electron Sink Facilitates Long-Term H₂ Photoproduction in Green Algae. *Biotechnol. Biofuels* **2019**, *12*, 280.
- (41) Englund, E.; Liang, F.; Lindberg, P. Evaluation of Promoters and Ribosome Binding Sites for Biotechnological Applications in the Unicellular Cyanobacterium *Synechocystis* Sp. PCC 6803. *Sci. Rep.* **2016**, *6*, 36640.
- (42) Thelwell, C.; Robinson, N. J.; Turner-Cavet, J. S. An SmtB-like Repressor from *Synechocystis* PCC 6803 Regulates a Zinc Exporter. *Proc. Natl. Acad. Sci. U. S. A.* **1998**, *95* (18), 10728–10733.
- (43) Kauny, J.; Sétif, P. NADPH Fluorescence in the Cyanobacterium *Synechocystis* Sp. PCC 6803: A Versatile Probe for *in vivo* Measurements of Rates, Yields and Pools. *Biochim. Biophys. Acta, Bioenerg.* **2014**, *1837* (6), 792–801.
- (44) Zaffagnini, M.; Fermani, S.; Marchand, C. H.; Costa, A.; Sparla, F.; Rouhier, N.; Geigenberger, P.; Lemaire, S. D.; Trost, P. Redox Homeostasis in Photosynthetic Organisms: Novel and Established Thiol-Based Molecular Mechanisms. *Antioxid. Redox Signaling* **2019**, *31* (3), 155–210.
- (45) Allahverdiyeva, Y.; Isojärvi, J.; Zhang, P.; Aro, E.-M. Cyanobacterial Oxygenic Photosynthesis Is Protected by Flavodiiron Proteins. *Life* **2015**, *5* (1), 716–743.
- (46) Feysa Özgen, F.; Runda, M. E.; Burek, B. O.; Wied, P.; Bloh, J. Z.; Kourist, R.; Schmidt, S. Artificial Light-harvesting Complexes Enable Rieske Oxygenase Catalyzed Hydroxylations in Non-photosynthetic Cells. *Angew. Chem., Int. Ed.* **2020**, *59* (10), 3982–3987.
- (47) Saroussi, S.; Karns, D. A. J.; Thomas, D. C.; Bloszies, C.; Fiehn, O.; Posewitz, M. C.; Grossman, A. R. Alternative Outlets for Sustaining Photosynthetic Electron Transport during Dark-to-Light Transitions. *Proc. Natl. Acad. Sci. U. S. A.* **2019**, *116* (23), 11518–11527.
- (48) Jensen, P. E.; Leister, D. Cyanobacteria as an Experimental Platform for Modifying Bacterial and Plant Photosynthesis. *Front. Bioeng. Biotechnol.* **2014**, *2*. DOI: 10.3389/fbioe.2014.00007
- (49) Sebesta, J.; Peebles, C. AM. Improving Heterologous Protein Expression in *Synechocystis* Sp. PCC 6803 for Alpha-Bisabolene Production. *Metab. Eng. Commun.* **2020**, *10*, No. e00117.
- (50) Hauf, W.; Schlebusch, M.; Hüge, J.; Kopka, J.; Hagemann, M.; Forchhammer, K. Metabolic Changes in *Synechocystis* PCC6803 upon Nitrogen-Starvation: Excess NADPH Sustains Polyhydroxybutyrate Accumulation. *Metabolites* **2013**, *3* (1), 101–118.
- (51) Zhou, J.; Zhang, F.; Meng, H.; Zhang, Y.; Li, Y. Introducing Extra NADPH Consumption Ability Significantly Increases the Photosynthetic Efficiency and Biomass Production of Cyanobacteria. *Metab. Eng.* **2016**, *38*, 217–227.
- (52) Mi, H.; Klughammer, C.; Schreiber, U. Light-Induced Dynamic Changes of NADPH Fluorescence in *Synechocystis* PCC 6803 and Its *NdhB*-Defective Mutant M55. *Plant Cell Physiol.* **2000**, *41* (10), 1129–1135.
- (53) Holland, S. C.; Kappell, A. D.; Burnap, R. L. Redox Changes Accompanying Inorganic Carbon Limitation in *Synechocystis* sp. PCC 6803. *Biochim. Biophys. Acta, Bioenerg.* **2015**, *1847* (3), 355–363.
- (54) Yao, L.; Shabestary, K.; Björk, S. M.; Asplund-Samuelsson, J.; Joansson, H. N.; Jahn, M.; Hudson, E. P. Pooled CRISPRi Screening of the Cyanobacterium *Synechocystis* sp PCC 6803 for Enhanced Industrial Phenotypes. *Nat. Commun.* **2020**, *11* (1), 1666.
- (55) Hoschek, A.; Bühler, B.; Schmid, A. Stabilization and Scale-up of Photosynthesis-driven Ω -hydroxylation of Nonanoic Acid Methyl

Ester by Two-liquid Phase Whole-cell Biocatalysis. *Biotechnol. Bioeng.* **2019**, *116* (8), 1887–1900.

(56) Heining, M.; Sutor, A.; Stute, S. C.; Lindenberger, C. P.; Buchholz, R. Internal Illumination of Photobioreactors via Wireless Light Emitters: A Proof of Concept. *J. Appl. Phycol.* **2015**, *27* (1), 59–66.

(57) Barbosa, M. J.; Janssen, M.; Ham, N.; Tramper, J.; Wijffels, R. H. Microalgae Cultivation in Air-Lift Reactors: Modeling Biomass Yield and Growth Rate as a Function of Mixing Frequency. *Biotechnol. Bioeng.* **2003**, *82* (2), 170–179.

(58) Hackenberg, C.; Engelhardt, A.; Matthijs, H. C. P.; Wittink, F.; Bauwe, H.; Kaplan, A.; Hagemann, M. Photorespiratory 2-Phosphoglycolate Metabolism and Photoreduction of O₂ Cooperate in High-Light Acclimation of *Synechocystis* sp. Strain PCC 6803. *Planta* **2009**, *230* (4), 625–637.

(59) Bulychev, A. A.; Cherkashin, A. A.; Muronets, E. M.; Elanskaya, I. V. Photoinduction of Electron Transport on the Acceptor Side of PSI in *Synechocystis* PCC 6803 Mutant Deficient in Flavodiiron Proteins Flv1 and Flv3. *Biochim. Biophys. Acta, Bioenerg.* **2018**, *1859* (10), 1086–1095.

(60) Klughammer, C.; Schreiber, U. Complementary PS II Quantum Yields Calculated from Simple Fluorescence Parameters Measured by PAM Fluorometry and the Saturation Pulse Method. *PAM Appl. Notes* **2008**, *1*, 27–35.

(61) Klughammer, C.; Schreiber, U. Saturation Pulse Method for Assessment of Energy Conversion in PS I. *PAM Application Notes* **2008**, *1*, 11–14.